The spectral extent of chorus in the off-equatorial magnetosphere

N. L. Bunch,[1] M. Spasojevic,[1] Y. Y. Shprits,[2,3,4] X. Gu,[5] and F. Foust[1]

Received 31 July 2012; revised 20 November 2012; accepted 29 November 2012.

[1] Magnetospheric chorus waves are a major driver of acceleration and loss in the Earth's outer electron radiation belt. The spectral extent of chorus is a key parameter in quantifying the global effect of chorus on energetic particle populations by determining the range of resonant electron energies. However, statistics of spectral properties are sparse, particularly in the off-equatorial magnetosphere. We use a database of chorus observations from the Polar spacecraft to generate statistics on the normalized chorus frequency (with the respect to the minimum field line gyrofrequency, Ω_{min}) as a function of magnetic local time (MLT) ($0 < MLT < 24$), L-shell ($3 < L < 11$), and magnetic latitude ($|\lambda| < 65°$). We find that, on average, the chorus spectrum peaks in the range of 0.1–0.4 Ω_{min}, varying significantly with λ, R_0 and MLT. The normalized chorus peak frequency is found to decrease with increasing R_0, and decreases with increasing latitude below $\sim 25°$. When fit to a Gaussian spectral model, lower band chorus is found to have a bandwidth < 0.1 Ω_{min}, which is narrower than assumed in most diffusion models. Diffusion coefficients calculated using the University of California at Los Angeles (UCLA) Full Diffusion Code show that wave-particle interactions on the nightside are highly sensitive to both the peak frequency and bandwidth of chorus, yet on the dayside scattering is mostly sensitive to the peak frequency as a result of the wider latitudinal extent of the waves. We also find that fitting a Gaussian to the logarithm of the spectrum reduces fit errors by over 60%, indicating that inclusion of arbitrary spectral forms may improve the accuracy of wave models within radiation belt simulations.

Citation: Bunch, N. L., M. Spasojevic, Y. Y. Shprits, X. Gu, and F. Foust (2013), The spectral extent of chorus in the off-equatorial magnetosphere, *J. Geophys. Res. Space Physics*, *118*, doi:10.1029/2012JA018182.

1. Introduction

[2] Chorus is a spontaneous electromagnetic whistler mode emission that is believed to play a major role in the evolution of energetic electron fluxes in the outer radiation belt through both energy and pitch angle scattering [*Thorne*, 2010]. Early spacecraft observations showed that the bandwidth of chorus scales as a function of the equatorial electron gyrofrequency (Ω_{min}), extending from ~ 0.05 to $0.8\,\Omega_{min}$ with a distinct gap in wave power typically observed near $0.5\,\Omega_{min}$ [*Burtis and Helliwell*, 1969, 1976; *Tsurutani and Smith*, 1977, 1977b]. For near equatorial emissions, *Burtis and Helliwell* [1976] reported that the center frequency of lower band chorus is located near $\sim 0.34\,\Omega_{min}$, but the peak in the wave power tends to occur at frequencies slightly below the center frequency in the range of ~ 0.15–$0.3\,\Omega_{min}$ [*Tsurutani and Smith*, 1977; *Santolik et al.*, 2005]. In the range of $4 < L < 6$, the peak frequency of lower band chorus tends to decrease with increasing latitude [*Burtis and Helliwell*, 1969; *Ni et al.*, 2011a, 2011b], an effect attributed to inward cross-L propagation [*Burtis and Helliwell*, 1969]. Possibly also due to propagation effects, the bandwidth of lower band chorus has been observed to increase slightly with latitude [*Burtis and Helliwell*, 1976; *Ni et al.*, 2011a]. Upper band chorus has a center frequency near $\sim 0.53\,\Omega_{min}$ [*Burtis and Helliwell*, 1976] and is on average 1 to 2 orders of magnitude weaker than lower band chorus [*Meredith et al.*, 2001; *Haque et al.*, 2010; *Li et al.*, 2011]. Unlike lower band chorus, which can extend out to the magnetopause on the dayside, upper band chorus tends to be confined to $L < 8$ [*Santolik et al.*, 2005; *Li et al.*, 2011] and $|\lambda| < 15°$ [*Meredith et al.*, 2001] with the latitudinal confinement attributed to the propagation of upper band chorus at higher wave normal angle and subsequent Landau damping [e.g., *Burton and Holzer*, 1974; *Haque et al.*, 2010].

[3] Accurate inclusion of the effects of wave-particle interactions driven by chorus into global diffusion models of the radiation belts requires statistical quantification of wave parameters [*Horne et al.*, 2005; *Summers*, 2005; *Shprits et al.*, 2006]. Combined with local plasma conditions and propagation angle, the spectral distribution of chorus is

[1]Space, Telecommunications, and Radioscience Laboratory, Stanford University, Stanford, California, USA.
[2]Department of Earth and Space Sciences, University of California, Los Angeles, California, USA.
[3]Department of Earth, Atmospheric and Planetary Sciences, Massachusetts Institute of Technology, Cambridge, Massachusetts, USA.
[4]Skolkovo Institute of Science and Technology, Moscow, Russia.
[5]Department of Atmospheric and Oceanic Sciences, University of California, Los Angeles, California, USA.

Corresponding author: N. L. Bunch, STAR Laboratory, Department of Electrical Engineering, Stanford University, 350 Serra Mall, Stanford, CA, 94305, USA. (nbunch@stanford.edu)

2169-9380/13/2012JA018182

required to determine the range of resonant electron energies and the resulting diffusion rates. Due to a prevalence of data in the region, chorus characteristics near the magnetic equator have been examined in detail [e.g., *Meredith et al*., 2001, 2003; *Li et al*., 2009, 2011]. However, on the dayside significant wave power can extend up to $|\lambda|>40$–50° [e.g., *Bunch et al*., 2011, 2012], and thus characterization of waves in this region is important for understanding the evolution of electrons in the 0.5–2 MeV range [*Thorne et al*., 2005]. Early work by *Tsurutani and Smith* [1977] examined the peak frequency of chorus in the high-latitude outer dayside magnetosphere. When normalized to the *local* gyrofrequency, two peaks were found both in the lower band, which the authors attributed to possible generation in high-latitude minimum-*B* pockets in addition to equatorial generation.

[4] In global radiation belt models, diffusion rates are typically determined using an approximation to the chorus spectrum modeled by a Gaussian of the form $B^2(\omega)=A\exp[-((\omega-\omega_m)/\delta\omega)^2]$, where $B^2(\omega)$ is the power spectral density of the chorus magnetic field (in nT ^{2}/Hz) as a function of wave frequency, A is a normalization constant proportional to the total wave power B_w^2, ω_m is the normalized frequency of maximum wave power, ω_{uc} and ω_{lc} are the upper and lower cutoffs, and $\delta\omega$ is the bandwidth [e.g., *Horne et al*., 2003].

[5] Values of each parameter can be tuned to represent specific chorus environments. Models including more than one Gaussian can also be used to model cases of strong upper and lower chorus bands together. Radiation belt diffusion due to chorus mostly depends on lower band parameters such that a single model of the lower band is often applied [e.g., *Shprits et al*., 2006, 2009]. Statistics compiled by *Burtis and Helliwell* [1976] and *Tsurutani and Smith* [1977] are typically used to determine ω_m, but less work has been done statistically to determine $\delta\omega$ or other parameters and their variability. Various values of these parameters are used in the literature, but the most commonly used model, referred to here as the "standard model", uses $\omega_m = 0.35$, $\delta\omega=0.15$, $\omega_{lc}=0.05$, and $\omega_{uc}=0.65$ [e.g., *Horne et al*., 2003, 2005; *Summers*, 2005; *Orlova and Shprits*, 2010]. Recent studies of the CRRES data set have parameterized these spectral characteristics for the dawn local time sector in the range of $4 < L < 6$ and $|\lambda|<15^\circ$ to understand the role of chorus in precipitating plasma sheet electrons and generating diffuse aurora [*Thorne et al*., 2007; *Ni et al*., 2011a, 2011b, 2011c].

[6] In this paper, we statistically characterize the spectral characteristics of chorus in the off-equatorial magnetosphere using the database of chorus spectral density elements derived by *Bunch et al*. [2011] using data from the Plasma Wave Instrument (PWI) Sweep Frequency Receiver (SFR) on board the Polar spacecraft ($\sim$ 8 h, $\sim 2\times 9R_E$, $\sim 90^\circ$ inclination, North Pole apogee). We find that, on average, the frequency of peak chorus intensity is in the range 0.1–0.4 Ω_{min}, and the bandwidth is in the range 0.04–0.09 Ω_{min}. The values of both parameters are lower than those widely used in quasi-linear diffusion models. The impact of these spectral parameters on diffusion rates is evaluated, and we show that the lower peak frequency and narrower bandwidth suggested by these data significantly impact scattering rates when waves are confined to $|\lambda|<15^\circ$. However when waves extend to higher latitudes (e.g., up to $|\lambda|=45^\circ$) scattering rates are predominantly sensitive to the peak frequency.

2. Spectral Distributions of Off-Equatorial Chorus

[7] The database of chorus power spectral density ($\omega-t$) elements is derived from the Polar PWI Sweep Frequency Receiver as described by *Bunch et al*. [2011, 2012], and includes chorus observations at frequencies $>$ 200 Hz, with frequencies resolved on a log scale, and a time resolution of $\sim$30 s. The SFR operated reliably in this mode from 25 March 1996 to 16 September 1997, a period of relative solar minimum beginning at the start of solar cycle 23. Chorus events were selected in frequency and time by visual inspection and filtered for electromagnetic signals using the SFR onboard correlator, which resulted in a database of electric and magnetic field measurements for individual chorus $\omega-t$ elements. Each $\omega-t$ element is normalized to Ω_{min} using the *Tsyganenko and Sitnov* [2005] magnetic field model and the *Qin et al*. [2007] solar wind database, and the elements are binned by radial distance of equatorial field line crossing (R_0) and magnetic latitude (λ). Figure 1 shows the spectral properties of equatorial $|\lambda|< 15^\circ$ (bottom) and off-equatorial $|\lambda|> 15^\circ$ (top) chorus separated by MLT sector (columns). Each panel accumulates $>$ 1080 32 s chorus intervals (equivalent to $>$ 576 min of chorus observations). The orbit of Polar results in observations near the equator to be limited to $3 <R_0< 5$ and off-equatorial observations to $R_0> 4$. Normalized $\omega-t$ elements are binned by 0.04 Ω_{min}.

[8] The blue curves are, given a chorus observation, the probability of observing chorus as a function of normalized frequency. The probability distribution peaks above $0.2\Omega_{min}$ in all sectors. For $\lambda< 15^\circ$ ($3 <R_0< 5$), the probabilities in all MLT sectors peak above 0.5 Ω_{min}, with chorus being 2–4 times more likely to reside in the upper band (>0.5 Ω_{min}) than in the lower band. For $\lambda> 15^\circ$ ($R_0> 4$), lower band chorus dominates at dawn, noon, and dusk, while at midnight the distribution is broader but still peaks in the lower band. We attribute this broadening at midnight to mapping uncertainty at off-equatorial latitudes.

[9] In comparing the local B_0 measured by Polar and the output of the *Tsyganenko and Sitnov* [2005] model, we find that the mean square error is highest in the midnight sector (3520 nT^2 mean squared error at midnight, 954 nT^2 for other sectors).

[10] The green curves are the mean value of the magnetic spectral density as a function of normalized frequency for all chorus events. The peak spectral density in all cases, with the exception of the midnight equatorial region, is located below 0.25 Ω_{min}.

[11] The expectation value of the chorus spectrum, plotted in red, is found by multiplying the mean spectral density (green) with the probability of occurrence (blue). The expectation value curves peak in the lower band for all latitudes and local times. Thus, despite upper band chorus having a higher occurrence rate near the equator, by up to a factor of four, the lower band contains significantly more wave power.

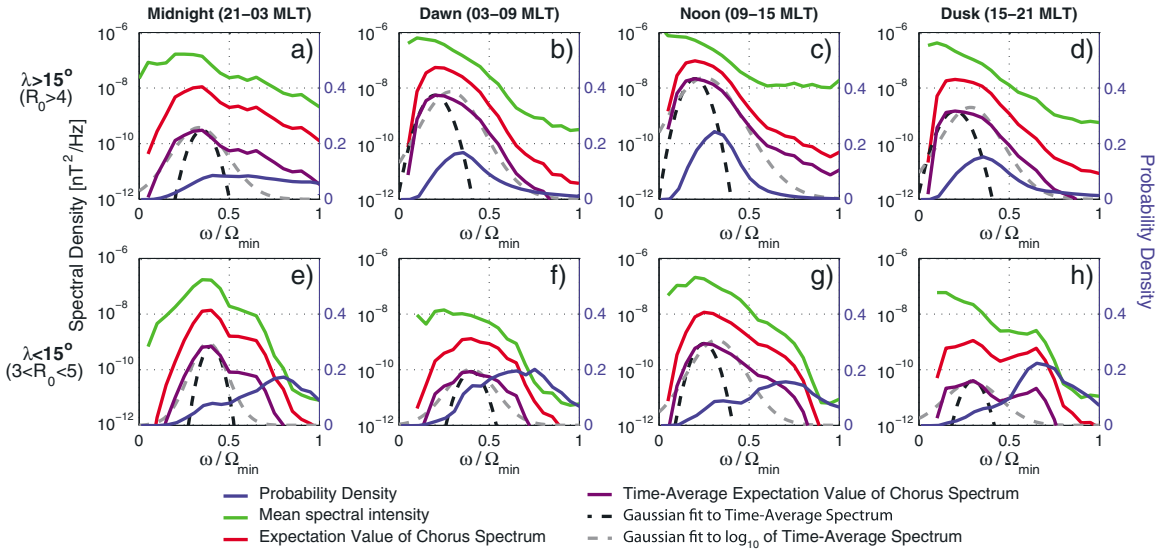

Figure 1. Chorus spectral properties. Mean spectral intensity (green), probability density (blue), expected power spectrum (red), and Gaussian fits to expected power spectrum for the midnight (21–03 MLT), dawn (03–09 MLT), noon (09–15 MLT), and dusk (15–21 MLT) sectors for (a–d) $\lambda > 15°$ and (e–h) $\lambda < 15°$.

[12] Also plotted in Figure 1 is the time-averaged expectation value (purple curves). This is found by multiplying the expectation value spectrum (red) by the fraction of time chorus is observed in each region. Hence, these curves show the same features as the expectation value spectra (red), but the wave power is reduced. For example, after adjusting for time-averaging, the chorus spectrum in the off-equatorial noon sector shows very little reduction with respect to the expectation value spectrum due to the high occurrence rate there, whereas the dusk sector, and off-equatorial midnight region see a large reduction in the time-averaged power spectrum by over an order of magnitude [cf. *Bunch et al.*, 2012].

[13] Black dashed lines shown in Figure 1 are Gaussian fits to the time-averaged expected power spectrum (purple curve) of the form shown in section 1. Fits to the power spectrum are concentrated in the lower band because expected power peaks there, and is thus the focus of this study. Fits to the spectral bandwidth, $\delta\omega$, are in the range of 0.04–0.09 Ω_{min} with a mean of 0.07 Ω_{min} and show no clear trend with respect to λ, R_0, or local time. These values are significantly narrower than the value of 0.15 Ω_{min} that is typically used in global diffusion models [e.g., *Horne et al.*, 2003; *Shprits et al.*, 2006; *Orlova and Shprits*, 2010]. For cases shown in Figure 1, the Gaussian fits systematically under-represent the total wave amplitude by 40–50%. When included in diffusion calculations this underestimate of chorus intensity away from the peak may significantly impact scattering rates (see section 4).

[14] Because chorus spectral intensities and integrated amplitudes appear to more closely follow a lognormal distribution, we suggest that a fit to the logarithm of the spectral distribution might be better suited to modeling the chorus power spectrum. Examples of this fit are shown in Figure 1 as dashed gray lines, and have bandwidths in the range 0.15–0.3 Ω_{min}. These fits under/over represent the total wave amplitude by $<$ 15%. Most current global radiation belt models only allow for inclusion of Gaussian spectra; however, this result indicates that the inclusion of additional spectral forms, potentially even arbitrary forms [e.g., *Ukhorskiy et al.*, 2010], would be more appropriate.

3. Peak Frequency Variation

[15] Next, we examine the variation of the peak chorus frequency as a function of R_0 and λ. For each chorus time interval, the normalized frequency of the peak spectral density is determined. These values are then binned by R_0 (1 R_E) and λ (5°). Within each $R_0 - \lambda$ bin, the value of maximum likelihood of ω_m is determined by fitting the data to a Weibull probability density distribution and taking the peak as the most likely value. The Weibull distribution was chosen because it provided a lower squared error than other common density functions. The shape parameter was restricted to $>$ 1, with exact shape and scale parameters determined by least squares. To elicit variation with respect to the λ for fixed R_0, we take ω_m as the value of maximum likelihood within a moving window, which is stepped in 2.5° increments. This moving window process is also done for fixed λ to elicit variation as a function of R_0, in increments of 0.5 R_E. A bin was considered statistically significant if it contained $>$ 200 chorus intervals (equivalent to $>$ 106.7 min of chorus observations).

[16] The top panels of Figure 2 show the variation of ω_m as a function of R_0 for the dayside (6–18 MLT, left) and nightside (18–6 MLT) sectors. In the range of $4.5 < R_0 < 8$, there is a general trend of decreasing ω_m with increasing R_0 for both the dayside and nightside sectors. On the dayside chorus extends farther in R_0 and λ, and in this region ω_m begins to increase again, which we attribute to the 200 Hz instrumental cutoff. This cutoff is shown in Figures 2a and 2b by solid gray lines representing dawn (6 MLT), and the dashed black lines representing noon (12 MLT) in Figure 2a and midnight (24 MLT) in Figure 2b. This indicates that

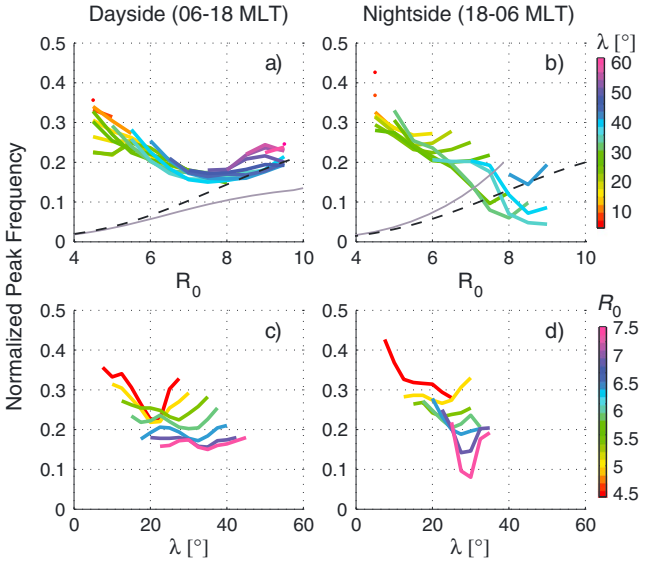

Figure 2. Chorus normalized peak frequency (Ω_m) as a function of R_0 and λ.

values of ω_m outside of $R_0 = 8$, where curves for ω_m intersect those for the instrumental cutoff, are deemed unreliable. As such, no curves for $R_0 > 8$ are shown in Figures 2c and 2d.

[17] Bottom panels of Figure 2 show the variation of ω_m with respect to λ. Again the dayside and nightside show similar trends where, for a fixed R_0, ω_m first decreases with increasing latitude up to $\sim 25°$ before increasing again. The location of the inflection point appears to be at higher latitudes for larger R_0, with more dramatic inflections occurring at higher latitudes on the dayside than on the nightside.

[18] To explain these features, we will consider both the initially generated spectral distribution and the evolution of the wave packets as they propagate. The feature of decreasing ω_m with increasing R_0 may be largely attributed to the radial variation of the ambient magnetic field and cold plasma density. Figure 3 shows the linear whistler mode growth rate as a function of normalized frequency for R_0 of 4 to 8 [*Kennel and Petschek*, 1966] calculated using a dipole magnetic field, which falls off as $1/r^3$, and a *Carpenter and Anderson* [1992] plasma trough density model at 6 MLT, which falls off as $1/r^4$. The hot plasma parameters are held constant with R_0, and we use a bi-Maxwellian distribution function with a loss cone depletion [*Katoh and Omura*, 2006] using $T_{||} = 26$ keV, $T_{\perp} = 36$ keV, a loss cone factor of 0.5, and a hot electron density of 0.25 cm^{-3}. These calculations show that the peak growth rate occurs at lower normalized frequency for higher values of R_0 and are consistent with the trend shown in Figure 2 (top row) of decreasing ω_m with increasing R_0. We note that the trend in Figure 3 is generally insensitive to the hot plasma parameters assuming the anisotropy is sufficient for growth.

[19] The propagation effects imposed on chorus wave packets may be more complex than the variation of initial growth conditions. For lower band chorus considered here, waves are typically initiated approximately field aligned [e.g., *Li et al.*, 2011] and will tend to propagate near this initial field line toward higher λ. As they propagate, waves may experience refraction, propagating inward or outward in R_0, as well as Landau damping, which is stronger for increasing wave normal angles. Thus, at lower λ the frequency distribution is primarily determined by the initial frequency distribution of the wave packet, and cross- R_0 propagation and Landau damping alter the distribution at higher λ. Past ray tracing studies have shown that inward or outward propagation depends strongly on frequency, density model, initial wave normal angle, initial R_0 and λ, and Landau damping rates [e.g., *Burtis and Helliwell*, 1969, 1976; *Bortnik et al.*, 2006, 2011]. In general, previous results point toward lower band chorus having greater tendency toward inward propagation, rather than outward [*Burtis and Helliwell*, 1969, 1976; *Santolik et al.*, 2006], which on average would lead to a decrease in ω_m with increasing λ, as was found here for $|\lambda| < 25°$. However, a comprehensive study using a realistic magnetic field model and Landau damping is required to truly test the global effect of off-equatorial chorus propagation, particularly for the outer dayside where complex magnetic field configurations can occur. A study of this nature is beyond the scope of the current investigation.

4. Impact of Chorus Spectra on Diffusion Time Scales

[20] To test the impact of chorus spectral properties on electron diffusion rates, we use the UCLA Full Diffusion Code [*Shprits et al.*, 2009]. For this calculation we assume $R_0 = 4.5$, chorus waves of 100 pT constant amplitude extending from the equator to $\lambda_{max} = \pm 45°$ for dayside chorus and $\lambda_{max} = \pm 15°$ for nightside chorus. The model outputs the bounce-averaged pitch angle ($D_{\alpha\alpha}$), momentum (D_{pp}), and mixed ($D_{\alpha p}$) diffusion coefficients as a function of equatorial pitch angle, α.

[21] Figure 4 shows example pitch angle and momentum diffusion curves for 100 keV electrons. Values of the pitch angle ($D_{\alpha\alpha}$) diffusion coefficient can be thought to represent the time required to deplete, in this case, the 100 keV electron population by a factor of $1/e$. Blue dashed lines are diffusion rates for the "standard" chorus spectral model, for which $\omega_m = 0.35$ and $\delta\omega = 0.15$.

[22] Comparing $D_{\alpha\alpha}$ for the standard model (blue dashed curves, Figures 4a–4b), we see that the high latitudinal

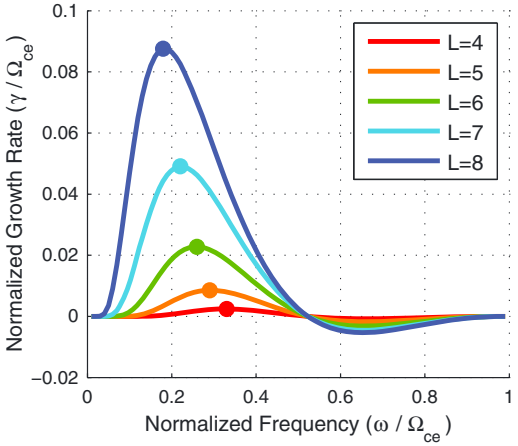

Figure 3. Linear whistler mode growth rate as a function of normalized frequency for R_0 of 4–8.

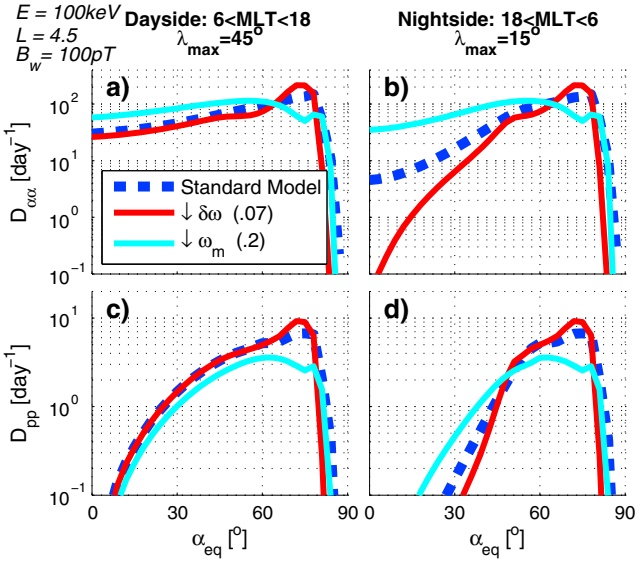

Figure 4. (a–b) Pitch angle and (c–d) momentum diffusion rates computed using the UCLA Full Diffusion Code for 100 keV electrons. The "standard" model assumes $\omega_m = 0.35$ and $\delta\omega = 0.15$, with cutoffs at $\omega_m \pm 2\delta\omega$, a reduced bandwidth model, with $\delta\omega = 0.07$, and a reduced frequency model with $\omega_m = 0.2$. Waves were extended to two different latitudes, 45° and 15°, to model the impact of dayside and nightside chorus waves, respectively.

extent of waves on the dayside results in scattering rates of almost an order of magnitude higher than on the nightside for small pitch angles (i.e., near the loss cone). Figures 4c and 4d show a similar effect on momentum diffusion rates in that dayside waves will energize a much broader range of the pitch angle distribution, with diffusion time scales for $\alpha = 30°$ decreasing from ~ 10 days to ~ 12 h from nightside to the dayside.

[23] Next, we compare diffusion rates when the bandwidth and peak frequency are reduced, such as was seen in the analysis of the Polar database above. The red curves in Figure 4 use the standard model with a reduced bandwidth of $\delta\omega = 0.07$, and the cyan curves use a reduced peak frequency of $\omega_m = 0.2$. On the dayside, varying the bandwidth and peak frequency has very little overall effect on the diffusion rates, with a slight increase in pitch angle diffusion at lower pitch angles for decreased peak frequency. However, on the nightside we see that the reduction in bandwidth results in a significant reduction in $D_{\alpha\alpha}$ and D_{pp} for $\alpha < 45°$.

[24] Finally, the reduction in peak frequency results in increased $D_{\alpha\alpha}$ near the loss cone for both dayside and nightside waves, and more variation in D_{pp} for the nightside than on the dayside.

[25] When considering the effect of varying chorus spectral features over a range of energies, we find that the general trend seen for 100 keV still holds, in that ω_m is the most significant spectral parameter for determination of diffusion rates on the dayside, whereas both ω_m and $\delta\omega$ can significantly affect nightside diffusion. Specifically though, for electrons in the MeV range, a reduced ω_m results in increased $D_{\alpha\alpha}$, where as reduced $\delta\omega$ has much less impact. At lower energies, in the tens of kiloelectron volt, electrons experience slower overall diffusion for reduced ω_m, and reduced $\delta\omega$ results in slower diffusion rates at high pitch angles.

5. Conclusions

[26] In this paper, we have used the *Bunch et al.* [2011] chorus database from the Polar spacecraft to analyze spectral properties of chorus as a function of MLT, R_0, and λ. Based on this work, the following primary conclusions have been made:

[27] 1. The probability of chorus as a function of frequency tends to peak at high fractions of Ω_{min}, while mean power spectral density as a function of frequency peaks at small fractions of Ω_{min}. This causes the peak of the time-averaged chorus spectrum to fall between these two values, and in the range of 0.1–0.4 Ω_{min}.

[28] 2. Chorus is observed 2–4 times more often in the upper band for $\lambda < 15°$ (orbitally constrained to $\sim 3 < R_0 < 5$). However, the total power content in the lower band is still 4–12 dB stronger in this region.

[29] 3. The wave power content of chorus for $\lambda > 15°$ is dominated by the lower band, often by several tens of decibels. This result is consistent with conclusion 2 above, and observations near the equatorial region [*Meredith et al.*, 2001], which indicate that chorus is globally strongest in the lower band (i.e., at all L and λ).

[30] 4. At fixed latitude λ, ω_m consistently decreases with R_0 for all time sectors. This result is consistent with whistler growth rate calculations, which show a shift in the peak growth rate toward lower normalized frequency with increasing R_0 simply as a result of the expected variation of density ($1/r^4$) and magnetic field strength ($1/r^3$) as a function of R_0.

[31] 5. At fixed R_0, ω_m tends to decrease with increasing λ. This result is generally consistent with previous observations by *Burtis and Helliwell* [1969] and *Ni et al.* [2011a]; however, a possible inflection toward higher ω_m at $\lambda > 25°$ is observed. This trend is likely the result of competing effects of wave growth/damping and propagation across field lines, and to sort out the competing factors will require extensive tray tracing simulation in realistic magnetic field geometries.

[32] 6. The bandwidth of chorus ($\delta\omega$) determined by Gaussian fit to the expectation value of the power spectrum ranges from 0.04 to 0.09 (~ 0.07 on average). No systematic variation of $\delta\omega$ was found with respect to R_0, λ, or MLT. This is lower than the widely adopted value of 0.15 used in most diffusion codes, and is on the low end of values 0.07–0.13 reported by *Ni et al.*, [2011a, 2011c].

[33] 7. Gaussian fits to the time-averaged power spectrum systematically under-represent the total wave amplitude by 40–50%, whereas Gaussian fits to the logarithm of the time-averaged power spectrum results in errors of < 15%. Thus, while most current global radiation belt codes only allow for inclusion of Gaussian spectra, inclusion of additional and potentially even arbitrary spectral forms would improve the accuracy of wave models within radiation belt simulations.

[34] 8 The peak frequency of chorus (ω_m) is the most significant parameter for determination of diffusion rates on the dayside, whereas both ω_m and $\delta\omega$ are significant for nightside diffusion.

[35] **Acknowledgments.** The OMNI data were obtained from the GSFC/SPDF OMNIWeb. We thank D. Boscher, S. Bourdarie, P. O'Brien, and T. Guild for providing the ONERA-DESP library V4.2, Toulouse-France, 2004-2008. We acknowledge PI, D. A. Gurnett, and The University of Iowa, for the Polar PWI data. This research was supported by the NASA Living With a Star Heliophysics Postdoctoral Fellowship Program, administered by the UCAR Visiting Scientist Programs, as well as NASA grant NNX09AF51G and NSF award 1043442.

References

Bortnik, J., U. S. Inan, and T. F. Bell (2006), Landau damping and resultant unidirectional propagation of chorus waves, *Geophys. Res. Lett.*, *33*, L03102, doi:10.1029/2005GL024553.

Bunch, N. L., M. Spasojevic, and Y. Y. Shprits (2011), On the latitudinal extent of chorus as observed by the Polar Plasma Wave Instrument, *J. Geophy. Res.*, doi:10.1029/2010JA016181.

Bunch, N. L., M. Spasojevic, and Y. Y. Shprits (2012), Off-equatorial chorus occurrence and wave amplitude distributions as observed by the Polar Plasma Wave Instrument, *J. Geophys. Res.*, *117*, A04205, doi:10.1029/2011JA017228.

Burtis, W. J., and R. A. Helliwell (1969), Banded ChorusÑA New Type of VLF Radiation Observed in the Magnetosphere by OGO 1 and OGO 3, *J. Geophys. Res.*, *74*(11), 3002–3010, doi:10.1029/JA074i011p03002.

Burtis, W. J., and R. A. Helliwell (1976), Magnetospheric chorus: Occurrence patterns and normalized frequency, *Planet. Space Sci.*, *24*(11), 1007–1024, doi:10.1016/0032-0633(76)90119-7.

Burton, R. K., and R. E. Holzer (1974), The Origin and Propagation of Chorus in the Outer Magnetosphere, *J. Geophys. Res.*, *79*(7), 1014–1023, doi:10.1029/JA079i007p01014.

Carpenter, D. L., and R. R. Anderson (1992), An ISEE/Whistler Model of Equatorial Electron Density in the Magnetosphere, *J. Geophys. Res.*, *97*(A2), 1097–1108, doi:10.1029/91JA01548.

Haque, N., M. Spasojevic, O. Santolik, and U. S. Inan (2010), Wave normal angles of magnetospheric chorus emissions observed on the Polar spacecraft, *J. Geophys. Res.*, *115*, A00F07, doi:10.1029/2009JA014717.

Horne, R. B., S. A. Glauert, and R. M. Thorne (2003), Resonant diffusion of radiation belt electrons by whistler-mode chorus, *Geophys. Res. Lett.*, *30*(9), 1493, doi:10.1029/2003GL016963.

Horne, R. B., R. M. Thorne, S. A. Glauert, J. M. Albert, N. P. Meredith, and R. R. Anderson (2005), Timescale for radiation belt electron acceleration by whistler mode chorus waves, *J. Geophys. Res.*, *110*, A03225, doi:10.1029/2004JA010811.

Katoh, Y., and Y. Omura (2006), A study of generation mechanism of VLF triggered emission by self-consistent particle code, *J. Geophys. Res.*, *111*, A12207, doi:10.1029/2006JA011704.

Kennel, C., and H. Petschek (1966), Limit on Stably Trapped Particle Fluxes, *J. Geophys. Res.*, *71*(1), 1–28.

Li, W., R. M. Thorne, V. Angelopoulos, J. Bortnik, C. M. Cully, B. Ni, O. LeContel, A. Roux, U. Auster, and W. Magnes (2009), Global distribution of whistler-mode chorus waves observed on the THEMIS spacecraft, *Geophys. Res. Lett.*, *36*, L09104, doi:10.1029/2009GL037595.

Li, W., J. Bortnik, R. M. Thorne, and V. Angelopoulos (2011), Global Distribution of Wave Amplitudes and Wave Normal Angles of Chorus Waves Using THEMIS Wave Observations, *J. Geophys. Res.*, *116*, A12205, doi:10.1029/2011JA017035.

Meredith, N. P., R. B. Horne, and R. R. Anderson (2001), Substorm dependence of chorus amplitudes: Implications for the acceleration of electrons to relativistic energies, *J. Geophys. Res.*, *106*(A7), 13,165–13,178.

Ni, B., R. M. Thorne, N. P. Meredith, Y. Y. Shprits, and R. B. Horne (2011a), Diffuse auroral scattering by whistler mode chorus waves: Dependence on wave normal angle distribution, *J. Geophys. Res.*, *116*, A10207, doi:10.1029/2011JA016517.

Ni, B., R. M. Thorne, N. P. Meredith, R. B. Horne, and Y. Y. Shprits (2011b), Resonant scaterring of plasma sheet electrons leading to diffuse auroral precipitation: 2. Evaluation for whistler mode chorus waves, *J. Geophys. Res.*, *116*, A04219, doi:10.1029/2010JA016233.

Ni, B., R. M. Thorne, Y. Y. Shprits, K. G. Orlova, and N. P. Meredith, (2011c), Chorus-driven resonant scaterring of diffuse auroral electrons in nondipolar magnetic fields, *J. Geophys. Res.*, *116*, A06225, doi:10.1029/2011JA016517.

Orlova, K. G., and Y. Y. Shprits (2010), Dependence of pitch-angle scattering rates and loss timescales on the magnetic field model, *Geophys. Res. Lett.*, *37*, L05105, doi:10.1029/2009GL041639.

Qin, Z., R. E. Denton, N. A. Tsyganenko, and S. Wolf (2007), Solar wind parameters for magnetospheric magnetic field modeling, *Space Weather*, *5*, S11003, doi:10.1029/2006SW000296.

Santolik, O., E. Macusova, K. H. Yearby, N. Cornilleau-Wehrlin, and H. S. K. Alleyne (2005), Radial variation of whistler-mode chorus: First results from the STAFF/DWP instrument onboard the Double Star TC 1 spacecraft, *Ann. Geophys.*, *23*, 2937–2942, doi:10.5194/angeo-23-2937-2005.

Santolik, O., J. Chum, M. Parrot, D. A. Gurnett, J. S. Pickett, and N. Cornilleau-Wehrlin (2006), Propagation of whistler mode chorus to low altitudes: Spacecraft observations of structured ELF hiss, *J. Geophys. Res.*, *111*, A10208, doi:10.1029/2005JA011462.

Shprits, Y. Y., R. M. Thorne, R. B. Horne, and D. Summers (2006), Bounce-averaged diffusion coefficients for field- aligned chorus waves, *J. Geophys. Res.*, *111*, A10225, doi:10.1029/2006JA011725.

Shprits, Y. Y., D. Subbotin, and B. Ni (2009), Evolution of electron fluxes in the outer radiation belt computed with the VERB code, *J. Geophys. Res.*, *114*, A11209, doi:10.1029/2008JA013784.

Summers, D. (2005), Quasi-linear diffusion coefficients for field-aligned electromagnetic waves with applications to the magnetosphere, *J. Geophys. Res.*, *110*, A08213, doi:10.1029/2005JA011159.

Thorne, R. M., T. P. O'Brien, Y. Y. Shprits, D. Summers, and R. B. Horne (2005), Timescale for MeV electron microburst loss during geomagnetic storms, *J. Geophys. Res.*, *110*, A09202, doi:10.1029/2004JA010882.

Thorne, R. M., Y. Y. Shprits, N. P. Meredith, R. B. Horne, W. Li, and L. R. Lyons (2007), Refilling of the slot region between the inner and outer electron radiation belts during geomagnetic storms, *J. Geophys. Res.*, *112*, A06203, doi:10.1029/2006JA012176.

Thorne, R. M. (2010), Radiation belt dynamics: The importance of wave-particle interactions, *Geophys. Res. Lett.*, *37*, L22107, doi:10.1029/2010GL044990.

Tsurutani, B., and E. Smith (1977), Postmidnight Chorus: A Substorm Phenomenon, *J. Geophys. Res.*, *79*(1), 118–127, doi:10.1029/JA079i001p00118.

Tsurutani, B., and E. Smith (1977), Two Types of Magnetospheric ELF Chorus and Their Substorm Dependences, *J. Geophys. Res.*, *82*(32), 5112–5128, doi:10.1029/JA082i032p05112.

Tsyganenko, N. A., and M. I. Sitnov (2005), Modeling the dynamics of the inner magnetosphere during strong geomagnetic storms, *J. Geophys. Res.*, *110*(A3), 10.1029/2004JA010798.

Ukhorskiy, A. Y., Y. Y. Shprits, B. J. Anderson, K. Takahashi, and R. M. Thorne (2010), Rapid scattering of radiation belt electrons by storm-time EMIC waves, *Geophys. Res. Lett.*, *37*, L09101, doi:10.1029/2010GL042906.